Amino Acids
https://doi.org/10.1007/s00726-021-02972-2

ORIGINAL ARTICLE

Improved pharmacokinetics and bone tissue accumulation of Angiotensin-(1–7) peptide through bisphosphonate conjugation

Ali Aghazadeh-Habashi[1,2] · **Sana Khajehpour**[1]

Received: 22 December 2020 / Accepted: 26 March 2021

Abstract

The renin–angiotensin system (RAS) has a central role in renal and cardiovascular homeostasis. Angiotensin-(1–7) (Ang1–7), one of the RAS active peptides, exerts beneficial effects through different mechanisms. These biological actions suggest that Ang1–7 is an effective therapeutic agent for treating various diseases associated with activated RAS. However, its short half-life and poor pharmacokinetics restrict its therapeutic utility. Our laboratory has successfully synthesized and characterized an Ang1–7 conjugate (Ang Conj.) with a prolonged half-life and improved pharmacokinetics profile. The Ang Conj. has been prepared by PEGylation of Ang1–7 and conjugation with a bisphosphonate using solid-phase peptide synthesis and characterized by HPLC and mass spectrometer. The compound's stability has been tested in different storage conditions. The bone binding capacity was evaluated using a hydroxyapatite assay. Pharmacokinetic and tissue distribution studies were performed using iodinated peptides in rats. Ang Conj. was synthesized with > 90% purity. Bone mineral affinity testing showed Ang Conj. exhibited significantly higher bone mineral affinity than Ang1–7. The Ang Conj. remained stable for more than a month using all tested storage conditions. The Ang Conj. demonstrated higher affinity to bone, a longer half-life, and better bioavailability when compared with the native peptide. These results support that conjugation of Ang1–7 with bisphosphonate enables it to utilize bone as a reservoir for the sustained delivery of Ang1–7 to maintain therapeutic plasma levels. High chemical stability and about five to tenfold prolongation of Ang Conj. plasma half-life after administrations into rats proves the effectiveness of our approach.

Keywords Renin-angiotensin system · Angiotensin-(1–7) · Conjugation · Bone-targeting · Pharmacokinetics · Tissue distribution

Introduction

The renin-angiotensin system (RAS) plays an essential role in renal and cardiovascular homeostasis. Its systemic actions include regulating blood pressure, fluid, and electrolyte balance (Carey and Padia 2018). Constitutively, the RAS that expressed both systematically and locally consists of two opposing arms. The classical arm consists of the angiotensin-converting enzyme (AEC)/Angiotensin (Ang) II /Ang II type 1 receptor (AT1R), which is responsible for physiological and pathological effects such as inflammation, vasoconstriction, cell proliferation, and fibrosis. The classical arm of the RAS can impose systemic or tissue toxicity when it is activated. In contrast, the protective arm composed of the ACE2/Ang1–7/Mas receptor results in anti-inflammatory (Gallagher et al. 2014), antifibrotic (Cook et al. 2010), anti-proliferative (Krishnan et al. 2013), and vasodilatory (Santos 2014) effects. The RAS activation plays an essential role in various inflammatory disease pathophysiology (Ko and Bakris 2018). The RAS has been studied as a target for therapeutic intervention in different pathological conditions. Prior to the discovery of ACE2, all interventional approaches for targeting the RAS were focused on ACE and Ang II, which resulted in the introduction of ACE inhibitors (ACEIs) and AT1R blockers (ARBs). However, the ACE2/Ang1–7/Mas receptor arm's importance in the

Handling Editor: M. S. Palma.

✉ Ali Aghazadeh-Habashi
habaali@isu.edu

[1] College of Pharmacy, Idaho State University, Pocatello, ID, USA

[2] Department of Biomedical and Pharmaceutical Sciences, College of Pharmacy, Idaho State University, Leonard Hall 212, Pocatello, ID 83209-8288, USA

Published online: 31 March 2021

RAS regulation has become increasingly evident (Iwanami et al. 2014). As one of the RAS active peptides, Ang1–7 exerts beneficial and protective effects through different mechanisms. Possessing such biological actions suggests the Ang1–7 peptide is an effective therapeutic agent for the treatment of various diseases with activated RAS etiology such as: renal (Silveira et al. 2013; Zhang et al. 2010) and cardiovascular diseases (De Mello et al. 2007; Loot et al. 2002; Sasaki et al. 2001), diabetes (Giani et al. 2012, 2009; Santos et al. 2010), arthritis (da Silveira et al. 2010), pulmonary diseases (Klein et al. 2013; Shenoy et al. 2014), Alzheimer's disease (Chen et al. 2017; Jiang et al. 2016), and cancer (Krishnan et al. 2013; Machado et al. 2001; Pham et al. 2013; Soto-Pantoja et al. 2009).

Commercially unavailable, Ang1–7's short half-life due to rapid systemic clearance and enzymatic degradation via proteolysis in the kidneys, liver, and blood circulation reduces its therapeutic value. Collectively, these vulnerabilities contribute to the peptide's poor pharmacokinetics and erratic bioavailability. Different approaches such as cyclization (Kluskens et al. 2009), substitution with non-natural amino acid (Wester et al. 2017), and complexation with β-cyclodextrin (Lula et al. 2007) have been tried to address the issue. We improved stability and prolonged its biological half-life by using a bone-targeting moiety attached to Ang1–7 peptide through a spacer. The objective of this novel approach was to synthesize and characterize the preclinical pharmacokinetics and tissue distribution profiles of Ang1–7 PEGylated bisphosphonate conjugate (Ang Conj.) in healthy rats. Pharmacokinetic properties of ^{125}I-Ang1–7 and ^{125}I-Ang Conj and their tissue distribution were examined after single intravenous (*i.v.*) bolus and subcutaneous (*s.c.*) injections.

Methods and materials

Materials

The 2-chlorotritylchloride resin, Fmoc-protected amino acids, solvents, and reagents needed for peptide synthesis were purchased from Aapptec (Louisville, KY, USA). Maleimidopropionyl polyethyleneglycol (PEG) NHS ester was purchased from Polypure AS (Oslo, Norway), and thiol-bisphosphonate was obtained from Surfactis Technologies (Angers, France). (Asn^1-Val^5) Ang II (internal standard), HPLC grade acetonitrile, methanol, and trichloroacetic acid (were purchased from Sigma Aldrich (St. Louis, MO). Phosphate-buffered saline (PBS) [pH 7.4] containing neither calcium nor magnesium was purchased from Genesee Scientific (EL Cajun, CA, USA), and acetate buffer one molar solution [pH 5.5] was purchased from Alfa Aesar (Ward Hill, MA, USA).

Methods

Peptide synthesis, conjugation, and characterization of Ang Conj.

The Ang Conj. was synthesized through a standard method of Fmoc-mediated solid-phase peptide synthesis using Aapptec Focus Xi peptide synthesizer (Louisville, KY, USA). As shown in the schematic synthesis illustration (Fig. 1), Ang1–7 peptide synthesis was initially started from the C-terminus of the heptapeptide sequence using 2-chlorotritylchloride resin. The resin was coupled with the proline, in its Fmoc-protected form (Fmoc-Pro-OH) and was the first amino acid in the sequence. The chain elongation was performed by removing the Fmoc group from the resin-attached amino acid and then adding the next Fmoc-protected amino acid (based on the sequence) until the entire peptide was synthesized. Then, while the peptide was attached to the resin, it was coupled with the maleimidopropionyl PEG NHS ester (as a spacer component) followed by thiol-BP. After synthesis completion, the conjugate was cleaved from the resin. The resultant conjugate was purified using semi-preparative HPLC and characterized by MALDI-TOF mass spectrometer (Health Sciences Center (HSC) cores, University of Utah). A US patent application for this innovative Ang Conj. synthesis has been filed.

In-vitro hydroxyapatite binding study

The bone mineral affinity of Ang Conj. was evaluated using a hydroxyapatite (HA) binding study according to a published protocol (Yewle et al. 2013) with some modifications. Briefly, 20 µg of Ang1–7 or an equivalent amount of Ang Conj. was mixed with 5 mg of HA powder in 750 µL of the binding buffer with various concentrations (double-distilled water (D.D.), 10 mM PBS [pH 7.4], 50 mM PBS [pH 7.4], and acetate buffer [pH 4.0]). Similarly, tubes containing an equivalent amount of Ang1–7 or Ang Conj. were mixed in corresponding buffers without HA and were used as a negative control. Mixtures were shaken gently at room temperature for 1 h and then were centrifuged at 10,000*g* for 5 min. The supernatant was separated and assayed for unbound drug, using a fluorescence spectrometer (λE_x 215 nm, λE_m 305 nm). The percentage of HA binding was calculated as (Intensity of control – the intensity of supernatants)/Intensity of control × 100%. Each experiment was measured in triplicate.

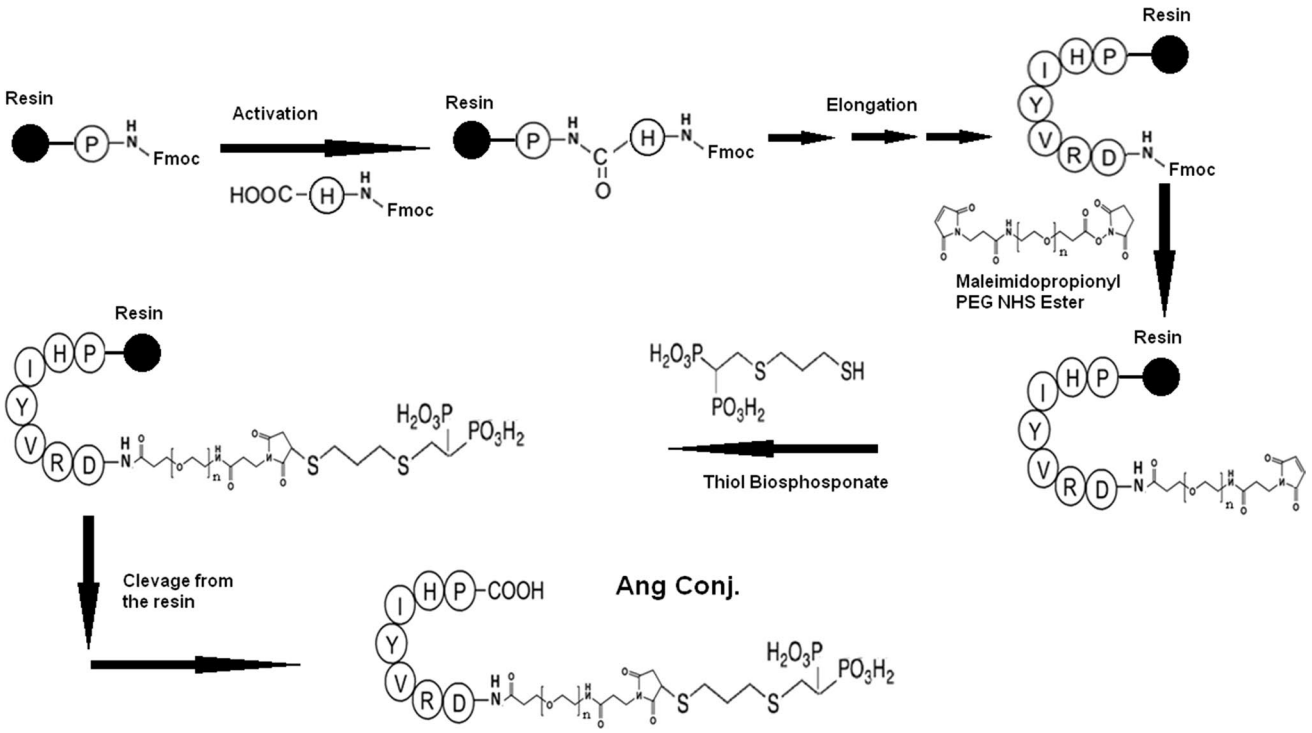

Fig. 1 Schematic illustration of Ang Conj. chemical synthesis using Fmoc-mediated solid-phase peptides

Analytical HPLC assay

An Agilent 1220 Infinity II HPLC system (Santa Clara, CA, USA), configured to include a degasser, a dual pump, an autosampler, a column oven, and a photodiode array detector, was used in this assay. Chromatographic separation was carried out using a Security Guard Cartridge Polar RP (KJ0-4282, 4.0 mm × 3.0 mm i.d.) and an Eclipse XRD-C18 analytical column (4.6 × 150 mm i.d. 5 µm,) purchased from Agilent Technologies (Santa Carla, CA, USA). The signal detection was monitored and integrated by the OpenLab CDS software version 2.2.0 from Agilent Technologies. The gradient mobile phase was composed of two solvents of A: H_2O/0.1% trifluoroacetic acid (TFA) and B: ACN/0.1% TFA. The mobile phase was delivered using a gradient elution program. The initial composition of the mobile phase ($t = 0$) was set at 10% B, which was increased linearly to 60% B over 5 min and then maintained at a plateau for additional 5 min. The gradient was then returned to 10% B over 3 min for column recalibration before the next sample injection. The sample run time was 13 min, and the column oven was set at 30 °C. The analytes were detectable at different wavelengths; however, 220 nm was chosen as the optimal wavelength for detection due to better sensitivity.

Validation of HPLC method

The HPLC method was validated for specificity, linearity, accuracy, and intra-day, and inter-day variations. The working calibration curves were prepared in three different mediums of double-distilled (D.D.) water, acetate buffer [pH 5.5], and PBS [pH 7.4] by serial dilution of the Ang1–7 and Ang Conj. stock solutions (500 µg/mL) and yielded standard samples containing 0.0, 50.0, 75.0, and 100.0 µg/mL of each compound. The standard curves were constructed by plotting the analyte/internal standard peak area ratio against each compound's given concentration. Three calibration curves were constructed on the same day or three different days to determine intra- and inter-day variabilities. The accuracy % was determined from observed concentration × 100/added concentration. The coefficient of variation (CV%) was used to estimate the assay precision (Table 1).

Stability study of Ang Conj.

Three different concentrations of 50, 75, and 100 µg/mL of Ang Conj. were prepared in DD water, acetate buffer [pH 5.5], and PBS buffer [pH 7.4] and stored at room temperature (25 °C), refrigerator (2–8 °C) and freezer (− 20 °C). After 1, 3, 7, 10, 15, and 30 days, 100 µL of the solutions

Table 1 Intra and inter-day precision (coefficient of variation, CV) and accuracy for HPLC assay of Ang Conj. in different mediums ($n=3$)

Medium	Con. (µg/mL)	Intra-day		Inter-day	
		(CV, %)	Accuracy (%)	(CV, %)	Accuracy (%)
D. D. Water	50.0	≤2.44	91.7 ± 6.7	≤0.99	99.6 ± 6.9
	75.0	≤1.31	101.1 ± 2.3	≤7.25	105.6 ± 12.6
	100.0	≤2.10	97.4 ± 2.7	≤6.23	106.8 ± 8.2
PBS buffer	50.0	≤2.81	91.5 ± 8.3	≤3.24	104.4 ± 12.6
	75.0	≤0.38	98.8 ± 0.7	≤8.37	107.8 ± 10.5
	100.0	≤2.90	100.7 ± 3.9	≤7.83	102.5 ± 10.4
Acetate buffer	50.0	≤1.53	94.3 ± 4.0	≤3.86	98.7 ± 11.5
	75.0	≤5.59	88.0 ± 10.2	≤10.36	102.7 ± 10.4
	100.0	≤1.05	99.3 ± 1.4	≤10.03	106.5 ± 10.1

was sampled and analyzed by HPLC–DAD to monitor the stability of Ang Conj. over time under different storage conditions.

Radiolabeling of Ang1–7 and Ang Conj.

The Ang1–7 and Ang Conj. were radiolabeled with $Na^{125}I$ according to the mild Iodogen method as previously described (Fraker and Speck Jr 1978) with some modification. Briefly, 40 µg (4.5 mM) of Ang1–7 or Ang Conj. equivalents were incubated with 0.1 mCi of $Na^{125}I$ in an Iodogen-coated tube pretreated with PBS [pH 7.4] for 30 min at room temperature with gentle shaking. The iodination yield was determined using radio-thin layer chromatography (R-TLC) with acetonitrile: water: TFA (60:40:0.1) as the mobile phase on Whatman paper #1. The iodinated peptides were separated and purified using a dialysis membrane (Spectrum ®, Gardena, CA, USA) with a cutoff point of 1000 and 3000 DMW for ^{125}I Ang1–7 and ^{125}I Ang Conj., respectively. The dialysis was performed using sterile and pyrogen-free PBS [pH 7.4] to remove and separate free ^{125}I from peptide-bound ^{125}I. The content of the dialysis sacs, including ^{125}I-Ang1–7 or ^{125}I-Ang Conj. were collected and quantified by R-TLC and used in pharmacokinetic studies.

Animals

The Idaho State University's Institutional Animal Care and Use Committee approved animal protocol (No. 760). Healthy Wistar rats (male) weighing 250–300 g were purchased from Simonsen Laboratories (Gilroy, California). Prior to any experimental procedure, the animals were acclimated for 4 days in the university animal facility, where all the studies were carried out. Two rats were housed in each cage in a room with controlled temperature (25 ± 1 °C), humidity (55 ± 5%), and a 12-h light/dark cycle. Animals had free access to a standard laboratory diet and water. After acclimatization, rats were randomly allocated to *i.v.*, and *s.c.* groups ($n=3$–4/group). Animals were anesthetized with oxygen/isoflurane and cannulated in the right jugular vein. After an overnight recovery, while under anesthesia, groups of animals were dosed with ^{125}I-Ang1–7 (*i.v.*) or ^{125}I-Ang Conj. (*i.v.* or *s.c.*) with a dose of 20 µg/kg peptide equivalent and the same activity of 10 µCi/kg through a jugular vein cannula, or *s.c.* injections. The cannula was flushed with the vehicle after dosing. Serial blood samples were collected at given time points. At 3 h post-dose, rats were euthanized by CO_2, and bone (tibia), brain, heart, kidney, liver, lung, muscle, testicle, and thyroid were collected. Residual blood was removed by rinsing with ice-cold PBS and blotted dry. Small pieces of each tissue were individually weighed, homogenized in 1 mL of TCA (10%, *v*/*v*), centrifuged, and the resultant pellets were collected.

Plasma and tissue homogenate samples were treated with ice-cold water 10% TCA. It precipitated intact iodinated Ang1–7 or Ang Conj. to eliminate any contribution to total activity originated from free ^{125}I or any ^{125}I associated with fragmented peptide. When ^{125}I-Ang1–7 or ^{125}I-Ang Conj. were incubated in vitro with blank rat plasma and tissue homogenate samples at 37 °C for up to 2 h, greater than 93% of the added radioactivity was recovered in the TCA precipitable pellets. Accordingly, the calibration standard curves were constructed by spiking the blank plasma and tissue homogenates with five concentrations (0–100 ng/mL) of radiolabeled peptides. The assay method was found to be linear over the range of tested concentrations with $r^2 > 0.99$ and accuracy > 90% for plasma and tissues (data not shown).

Pharmacokinetics and tissue distribution

Three rats received ^{125}I-Ang1–7 administered as a single *i.v.* bolus injection in PBS [pH 7.4] through a catheter. The other two groups received an equivalent dose of ^{125}I-Ang Conj. as a single *i.v.* bolus ($n=4$) or *s.c.* ($n=3$) injection. Rats in the *i.v.* groups were dosed through the cannula. After administration, 0.2 mL of saline used to flush out the tube. For *s.c.* group, the dose was delivered through a single *s.c.* injection at the nape of the neck.

Blood samples (~200 µL) were collected from the cannula into heparinized tubes before dosing and 5, 10, 15, 30, and 45 min and 1, 1.5, 2, and 3 h after administration. Blood samples were immediately processed, and plasma was then harvested by centrifugation at 8000 rpm and 4 °C for 10 min. The radioactivity in 100 µL aliquot of the plasma samples was determined after Ang1–7 peptide or its conjugate was precipitated by vortex-mixing with 0.9 mL of TCA (10%, *v*/*v*). The mixtures were incubated on ice for 30 min and centrifuged at 8000 rpm and 4 °C for 10 min. Then the supernatant, holding free ^{125}I or ^{125}I associated with smaller fragments of peptides, was aspirated. Consequently, the radioactivity of the resultant TCA precipitated pellet associated with ^{125}I-Ang1–7 or ^{125}I-Ang Conj. was measured using a Cobra TM Gamma Counting System (Packard Instrument Company Meriden, CT, USA) and used to determine their concentration.

At the end of the experiment, the anesthetized rats in the different groups were euthanized in a CO_2 chamber at 1.5 h (*i.v.* groups) and 3 h (*s.c.* group) post-dosing; and the tissues or organs were then removed. The small pieces of tissues were homogenized in ice-cold PBS [pH 7.4], and radiolabeled peptides were precipitated with TCA (10%, *v*/*v*). Then, the radioactivity was measured in pellets after centrifugation. The results were expressed as the percent of the total injected dose/gram of tissue or organ.

Pharmacokinetic modeling and analysis

Pharmacokinetic indices of ^{125}I-Ang1–7 and ^{125}I-Ang Conj were determined using non-compartmental analysis (WinNonlin version 4.0, Pharsight, A Certara Company, CA, USA). Doses were normalized based on animal body weight. The terminal elimination rate constant, K_e, for the iodinate peptides concentration–time curve after *i.v.* administration was determined by the linear regression of at least three data points from the terminal portion of the plasma concentration–time plots. The terminal half-life calculated based on $t_{1/2} = 0.693/K_e$. The area under the plasma concentration–time curve (AUC_t) was calculated using the trapezoidal rule until the last measured plasma concentration, C_{last}. The $AUC_{0\text{-}\infty}$ was calculated by adding up the AUC_t and C_{last}/K_e. The total body clearance, CL, was determined by *i.v.* dose divided by $AUC_{i.v.}$ The terminal phase volume of distribution of the compounds was calculated from $V_d = CL/K_e$. The Ang Conj. total body clearance and volume of distribution were corrected for bioavailability after s.c. injection, and presented as Cl/F and V/F, respectively. The parameters were determined for each animal, and the sample population averages were calculated. The observed peak plasma concentration (C_{max}) and the time-to-peak concentration (T_{max}) were recorded. Absolute bioavailability (*F*%) was calculated as (mean $AUC_{s.c.}$/mean $AUC_{i.v.}$) × (dose *i.v.*/dose *s.c.*) × 100.

Statistical analysis

All the data are expressed as mean (standard deviation). One-way analysis of variance (ANOVA) followed by Bonferroni adjustment was used to test the significant ($p < 0.05$) difference on tissue distribution of iodinated peptides between groups using GraphPad Prism® statistical software program version 3.0 (GraphPad Prism Software Inc., San Diego, CA).

Results

Synthesis of Ang Conj., HPLC-Isolation and characterization

Ang Conj. was synthesized successfully using solid-phase peptide synthesis (Fig. 1), isolated by HPLC (Fig. 2a), and confirmed by MALDI-TOF (Fig. 2b).

The synthesis resulted in a single conjugate with a molecular weight of 2650.1 Dalton. The representative HPLC–UV chromatogram of Ang Conj. shows a single peak with more than 90% purity (Fig. 2a). The MALDI-TOF mass spectrum presents negative ion: $m/z = 1324.24$ (M^{-2H+}), confirming Ang Conj's expected mass. (Fig. 2b).

Stability of Ang Conj.

The stability of the Ang Conj. was tested in three different matrixes of D.D. water, acetate buffer [pH 5.5], and PBS [pH 7.4]. This test was conducted at three temperature storage conditions: (1) room temperature (25 °C), (2) refrigerator (2–8 °C), and (3) freezer (− 20 °C), for 4 weeks to ensure that the conjugate did not degrade throughout the study. The results indicate that Ang Conj. is more stable in the acidic medium at all three storage conditions over 4 weeks (Table 2). The representative chromatograms show the peaks of internal standard, Ang Conj. and Ang1–7 after 28 days of storage in various matrixes and conditions (Fig. 3).

Bone targeting capacity through in vitro HA binding studies

The bone mineral affinity of bone-targeting Ang Conj. was tested and compared with the plain Ang1–7 peptide. As it shown in Fig. 4, Ang1–7 exhibited 4.2 ± 0.1%, 3.7 ± 0.6%, 4.4 ± 0.2%, and 2.6 ± 0.4% binding capacity in D.D. water, PBS 50 mM, PBS10mM, and acetate buffer, respectively. In contrast, those values for Ang Conj. were 20.4 ± 0.5%,

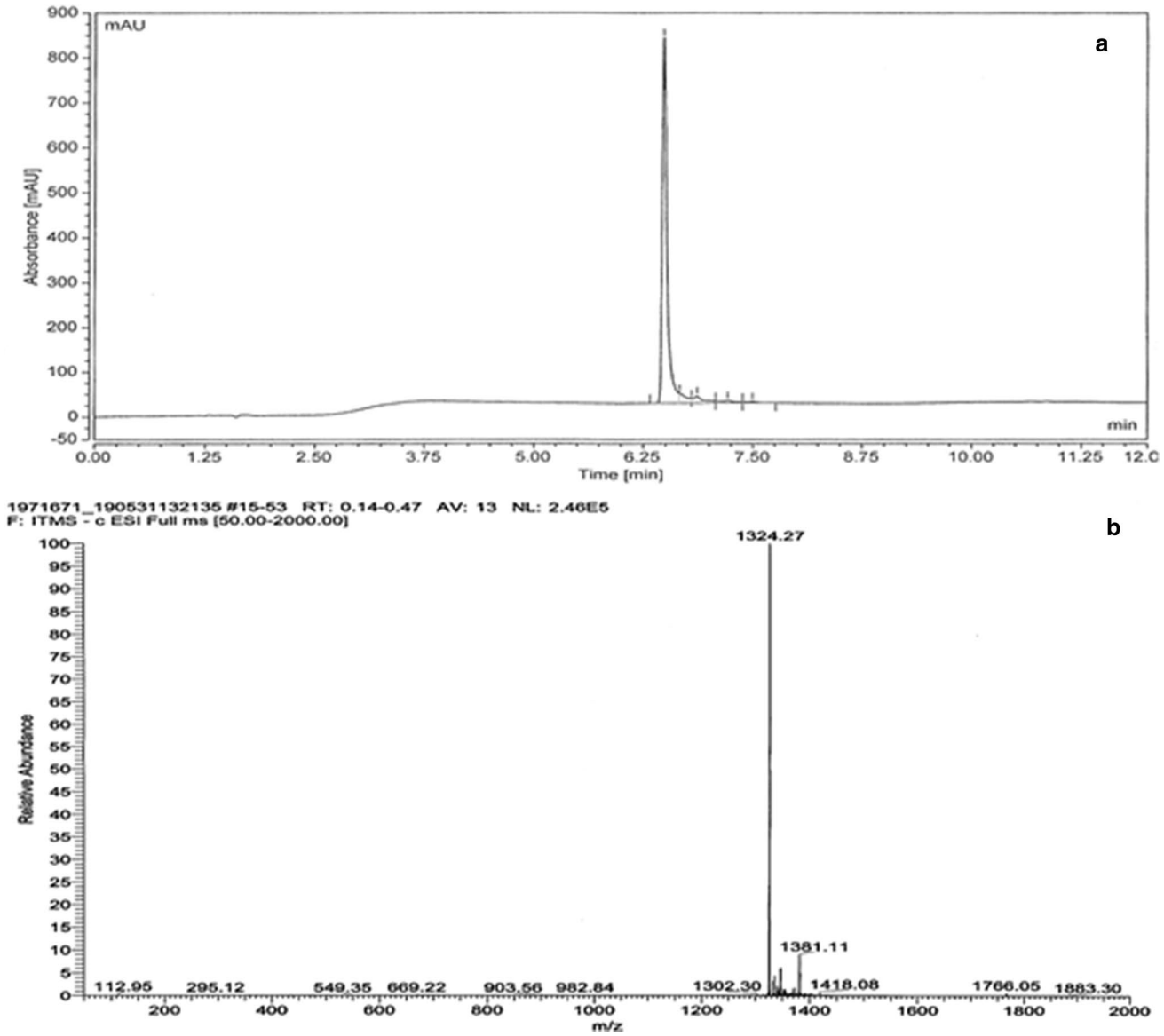

Fig. 2 Semi-Prep HPLC chromatogram (**a**) and MALDI-TOF mass spectrum of Ang Conj. (**b**)

Table 2 Percentage of Ang Conj. remaining after 4 weeks of storage in different mediums

Length of storage (day)	25 °C		4 °C		− 20 °C	
	5	28	5	28	5	28
Acetate buffer [pH 5.5]	94.3	93.3	98.4	98.0	99.8	99.5
D. D. Water [pH 6.5]	90.6	64.0	95.9	92.4	99.5	99.1
PBS buffer [pH 7.4]	72.8	22.6	91.9	79.2	99.2	98.9

6.8 ± 0.6%, 8.4 ± 0.2%, and 11.6 ± 0.2%. These data indicate that Ang Conj.'s binding capacity in each medium was significantly higher than Ang1–7. The binding capacity was additionally affected by the pH and phosphate ion presence and concentration. The acidic pH (pH 5.5 vs. pH 7.4) and a lower concentration of phosphate ion (10 mM vs. 50 mM) resulted in higher binding (Fig. 4).

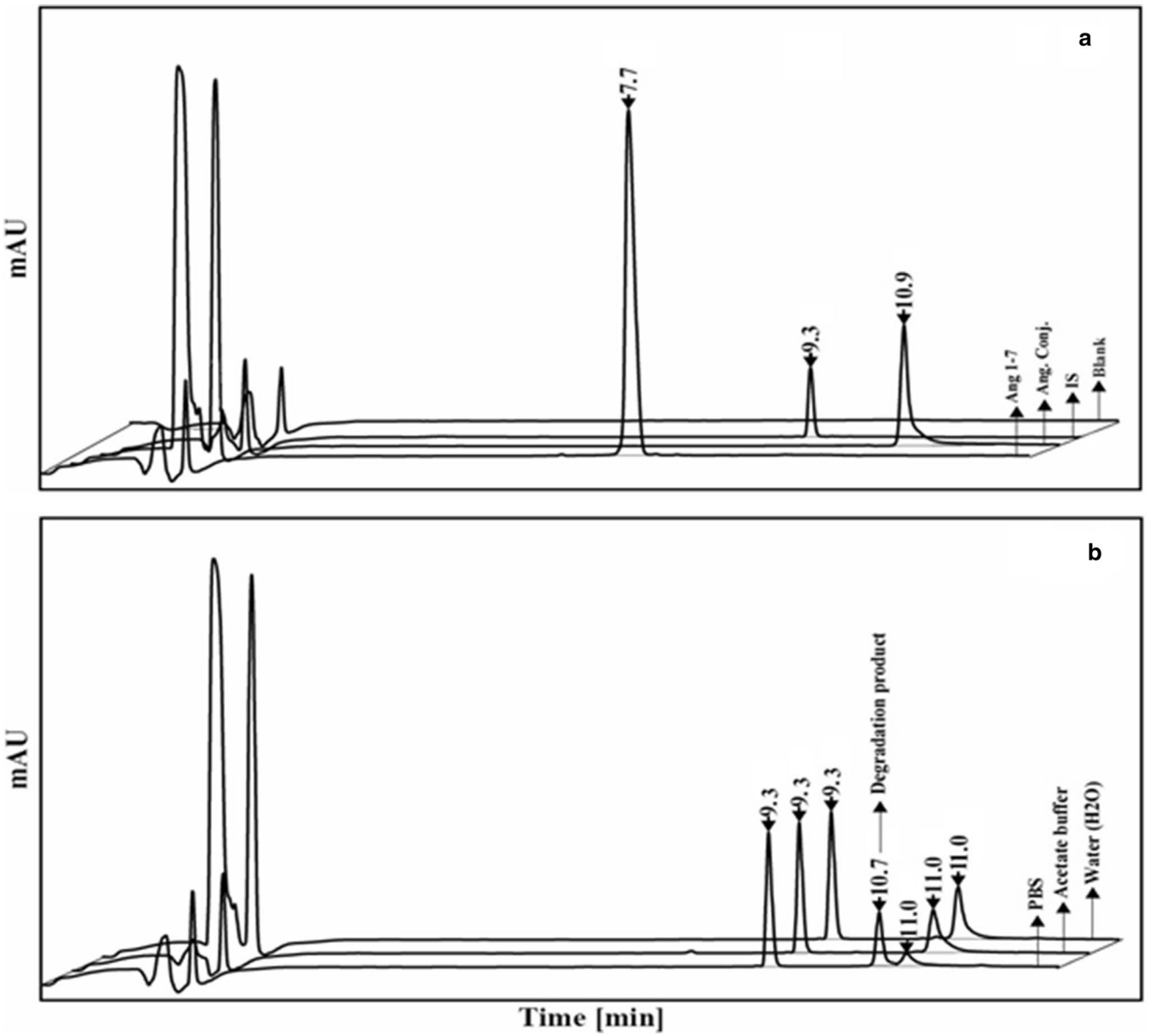

Fig. 3 Representative analytical HPLC–PDA individual chromatograms of **a** Blank, internal standard (IS), Ang1–7, and Ang Conj. standard solutions and **b** Ang Conj. solution (plus IS) in the different mediums after 28 days at room temperature

Radiolabeling

The radiolabeling process yield for ^{125}I-Ang1–7 or ^{125}I-Ang Conj. was 45 and 38%. Furthermore, the harvested ^{125}I-Ang1–7 or ^{125}I-Ang Conj. was more than 93% precipitable with TCA (10%, *v*/*v*) in blank rat plasma. The ^{125}I labeled Ang1–7 or ^{125}I-Ang Conj. fractions were mixed with unlabeled cold peptides in 50 mM PBS (pH 7.4) to achieve the final mixture peptide solutions for dosing used in animal experiments.

Pharmacokinetic studies

The corresponding non-compartmental pharmacokinetic parameters of ^{125}I-Ang1–7 and ^{125}I-Ang Conj. are listed in Table 3. After *i.v.* administration, both ^{125}I-Ang1–7 and ^{125}I-Ang Conj. declined in a multi-exponential fashion with a rapid initial distribution phase followed by a slower elimination phase (Fig. 5a).

Absorption of ^{125}I-Ang Conj. after *s.c.* administration was rapid, as indicated by the occurrence of mean peak plasma concentrations in about 0.3 ± 0.1 h (Fig. 5b and Table 3). There was a significant difference in mean values of $t_{1/2}$,

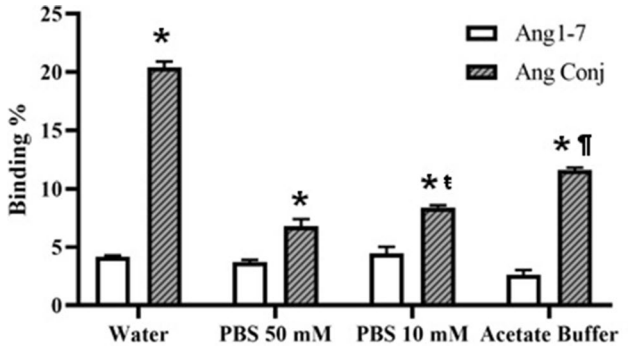

Fig. 4 The binding capacity of Ang1–7 and Ang Conj. in the different mediums. *Significantly different from Ang1–7, $p<0.01$, ŧsignificantly different form PBS 50 mM, $p<0.05$ ¶significantly different form PBS and water, $p<0.01$

Vd, CL, and AUC values following *i.v.* of ^{125}I-Ang1–7 and ^{125}I-Ang Conj. The PK parameters were significantly further increased ($t_{1/2}$ and AUC) or decreased (CL) after *s.c.* injection of ^{125}I-Ang Conj. when compared with *i.v.* route demonstration of ^{125}I-Ang1–7. The absolute bioavailability (*F*%) for *s.c.* dose was almost %118.6ŧ (Table 3).

Tissue distribution studies

Tissue distribution of ^{125}I-Ang1–7 and ^{125}I-Ang Conj. were studied with the same groups of rats at the end of experiment 3 h following single-dose administration through either *i.v.*, or *s.c.* routes. The data in Fig. 6 detail the percent of injected dose per gram of tissue or organ. The results indicated that the iodinated-peptides were widely distributed and accumulated in the tissues/organs throughout the whole body after 3 h. The tissue distribution of radioactivity following a single *i.v.* injection of ^{125}I-Ang–7 or ^{125}I-Ang Conj. were similar in all tested tissues other than bone tissue. A significant bone tissue radioactivity was observed after ^{125}I-Ang Conj.

Table 3 Pharmacokinetic parameters of ^{125}I-Ang1–7 and ^{125}I-Ang conj. After *i.v.* or *s.c.* Adminsitration in rats

PK Parameters	^{125}I-Ang1–7 (*i.v.*)	^{125}I-Ang Conj. (*i.v.*)	^{125}I-Ang Conj. (*s.c.*)
C_{max} (ng/mL)	–	–	131.0 (105.2)
T_{max} (h)	–	–	0.3 (0.1)
$t_{1/2}$ (h)	0.6 (0.1)	3.4 (1.4)[a]	6.6 (0.8)[a,b]
K_e (1/h)	1.1 (0.2)	0.2 (0.1)[a]	0.1 (0.0)[a,b]
V_d (mL)	22.3 (1.9)	35.7 (6.3)[a]	–
CL (mL/h)	24.2 (2.1)	6.1 (2.9)[a]	–
V_d/F (mL)	–	–	34.5 (5.0)[a]
CL/*F* (mL/h)	–	–	3.6 (0.4)[a,b]
AUC_t (ng*h/ mL)	21.2 (4.9)	124.6 (82.6)[a]	188.2 (45.8)[a]
AUC_{inf} (ng*h/ mL)	26.1 (6.4)	391.8 (158.1)[a]	464.7 (40.7)[a]
F%			118.6

[a]Significantly different from ^{125}I-Ang1–7, $p<0.05$, [b]Significantly different from ^{125}I-Ang Conj., $p<0.05$

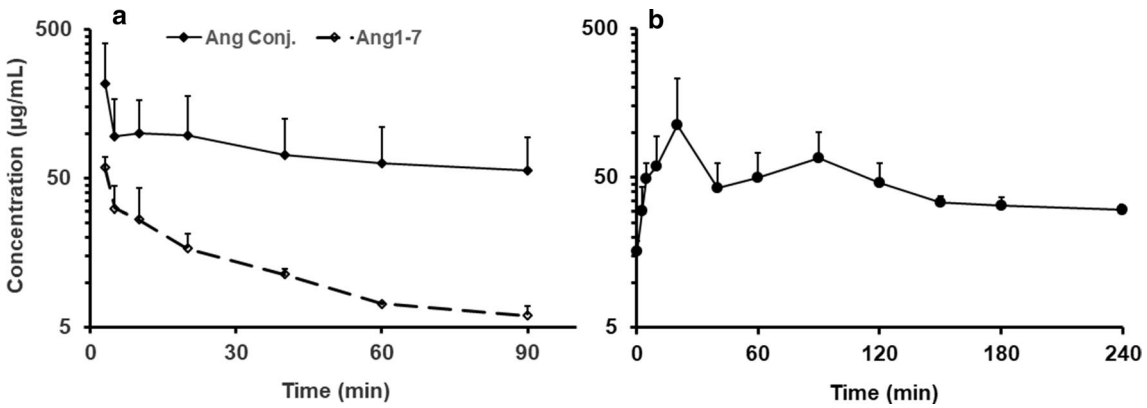

Fig. 5 Mean plasma concentration–time profile of ^{125}I-Ang1–7 ($n=3$) and ^{125}I-Ang Conj. ($n=4$) after *i.v.* (**a**) and ^{125}I-Ang Conj. ($n=3$) after *s.c.* adminsitration (**b**) in rats

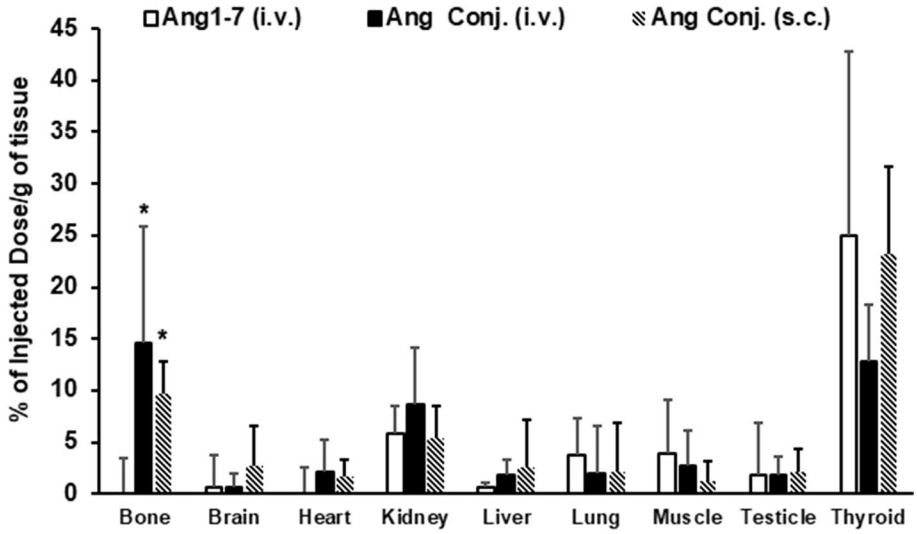

Fig. 6 The tissue distribution after *i.v.,* or *s.c.* administartion of ^{125}I-Ang1–7 ($n = 3$) and ^{125}I-Ang Conj. ($n = 3$–4/group) in rats, *significantly different from Ang1–-7, $p < 0.05$

administration and it was 14.1 ± 11.3% and 9.7 ± 3.2% after *i.v.* and *s.c*. injections, respectively. However, in ^{125}Ang1–7 treated rats, the activity was not significantly different from background readings.

Discussion

A short biological half-life and stability remain the primary challenge to biologically active peptides' recognition as promising therapeutic agents. Ang1–7, as an active peptide with several beneficial effects, is not an exception. Some recent clinical trials have applied the Ang1–7's beneficial effects for treating different pathological conditions by administering through a continuous infusion delivery method to avoid such restrictions (Petty et al. 2012, 2009; Rodgers and Oliver 2006). Also, several attempts have been made to improve peptide therapeutics, particularly Ang 1–7 stability, including PEGylation (Hamidi et al. 2006; Jevševar et al. 2010), cyclization (Kluskens et al. 2009), and *β*-cyclodextrin inclusion (Lula et al. 2007). In the current study, we synthesized a stable PEGylated bone-targeting conjugate of Ang1–7 while preserving its biological activity (Habashi et al. 2020).

The Ang Conj. presents with higher stability in different matrixes and longer biological half-life when compared with native Ang1–7 peptide. In contrast to in-solution synthesis, the multi-step solid-phase peptide synthesis approach coupled with subsequent PEGylation and conjugation with BP yields a pure (> 95%) compound (Fig. 2a). The MALDI-TOF spectrum of the resultant compound matches the expected molecular weight and confirms the successful synthesis of the conjugate (Fig. 2b). PEG utilization as a spacer in the conjugate structure resulted in higher stability (Table 1; Fig. 3). The HA binding study indicates that exposure of Ang conj. to HA in different mediums resulted in higher bone targeting efficacy (Fig. 4). Ang Conj. displayed more than fourfold higher bone HA binding capacity when compared with plain Ang1–7 in D.D. water [pH 6.0]. Its affinity declined from 20% to 11.6% when the pH was lowered from 6 to 4 (acetate buffer pH 4). However, the binding capacity was still higher when compared with PBS solutions with pH 7.4. The phosphate group's ionization status on the BP moiety and the presence of competing phosphate ions could explain the bone binding capacity of the conjugate in different mediums. The impact of competing ions was more evident when phosphate buffers with different molarity were used. The HA binding data (Fig. 4) indicate that the presence of competing phosphate ions in the matrix has more impact than pH and the ionization state of phosphate groups of the BP moiety on the conjugate HA binding.

The listed PK parameters of ^{125}I-Ang1–7 and ^{125}I-Ang Conj. after single *i.v.* and *s.c.* in Table 3 indicate that PEGylation and BP conjugation increased conjugate V_d and $t_{1/2}$ while decreasing its total body CL. The tissue distribution of bone-targeting ^{125}I-Ang Conj. specifies that after *i.v.* and *s.c.* injection, the most abundant radioactivity was detected in the bone tissue followed by thyroid, kidney, and muscle tissues. Only bone tissue showed a significant tissue distribution difference between^{125}I-Ang1–7 and ^{125}I- Ang Conj. The Ang Conj.'s higher bone binding capacity justifies the observed increased V_d. Besides, the limited distribution to other tissues can be explained by its increased hydrophilicity compared to Ang1–7. Although the liver and kidney tissue distribution was similar for native peptide and conjugate, the reduced exposure of hydrophilic conjugate to the liver and kidney enzymes could explain the significant reduction in total CL and $t_{1/2}$ prolongation. By the same token, significantly higher bone tissue binding validates the extended body exposure and increased total AUC. The

complete bioavailability of Ang Conj. suggests that it is sufficiently stable to be absorbed fully following *s.c.* dosing.

The roles played by the RAS's counter-regulating arms and their contribution to various pathological conditions continue to unfold, making the system an attractive drug development target. Previously overlooked by ACEIs and ARBs, the protective arm's triad of ACE2/Ang1–7/Mas receptor has gained considerable attention. Numerous studies have investigated the Ang1-7 peptide to determine its beneficial effects on counterbalancing the Ang II's negative impacts associated with activated RAS on cardiovascular (De Mello et al. 2007; Loot et al. 2002; Sasaki et al. 2001), renal (Silveira et al. 2013; Zhang et al. 2010), and pulmonary (Klein et al. 2013; Shenoy et al. 2014), arthritis (da Silveira et al. 2010), cancer (Krishnan et al. 2013; Machado et al. 2001; Pham et al. 2013; Soto-Pantoja et al. 2009), diabetes (Giani et al. 2009, 2012; Santos et al. 2010), and neurological disorders (Chen et al. 2017; Jiang et al. 2016; Kangussu et al. 2013). The Ang1–7 peptide acts through the Mas receptor and delivers an anti-inflammatory effect by inhibiting cytokine expression and release, reducing macrophage activation, and blocking fibrosis (da Silveira et al. 2010; El-Hashim et al. 2012; Jiang et al. 2012; Souza and Costa-Neto 2012).

We investigated the anti-proliferative and anti-inflammatory effects of Ang1–7 and Ang Conj. through in vitro and in vivo studies. The in vitro study results indicate that conjugation of Ang1–7 did not affect its biological activity and, due to improved stability, it significantly inhibited the cancer cells proliferation. This observation could be explained by increased gene expression of the ACE2 enzyme and Mas receptor. In an in vivo study, using a synovial sarcoma mouse model, the Ang Conj. presented with higher efficacy than Ang1–7 on suppressing the cancer progression, which translated into a significant tumor size reduction. This effect could be attributed to switching the balance between the RAS arms in favor of the protective arm with anti-proliferation, anti-angiogenesis, vasodilation, and anti-inflammation effects (unpublished data). We also studied the anti-inflammatory effects of the Ang Conj. and compared it with Ang1–7 in an adjuvant arthritis animal model. The joint bone is the most common tissue impacted by rheumatoid arthritis, targeting the bone with Ang Conj. could effectively control the signs and symptoms of experimental adjuvant arthritis. Daily *s.c*. administration of Ang1–7 or Ang Conj. for three weeks was able to alleviate the adjuvant arthritis signs and symptoms in rats. The anti-inflammatory effect was manifested by restoring the body weight gain, diminishing paws and joints' swelling, and reducing plasma nitric oxide levels. Furthermore, the inflammation-induced ACE2/ACE imbalance was corrected by Ang1–7 and Ang Conj. treatment (Habashi et al. 2020).

Strength and limitations of the work

This work is a novel approach to improve the stability, pharmacokinetics, and bone tissue accumulation of Ang1–7 peptide. This approach could potentially offer a reliable treatment option for various pathological conditions associated with the activated RAS. The general limitation of any pharmacokinetics and tissue distribution study using radiolabeled material is the lack of accurate discrimination between the radiation originated from free radiolabel and its bond form. In this study, we took an extra step to precipitate the ^{125}I-Ang1–7 or ^{125}I-Ang Conj using TCA and separate them from free iodine or small peptide labeled fragments accurately. Nevertheless, as future studies, we plan to confirm our findings by repeating this animal study result using unlabeled materials and detecting the intact Ang1–7 peptide or Ang Conj. by developing a validated LC–MS/MS method.

Conclusion

These results support the notion that the conjugation of Ang1–7 with bone-seeking BP enables Ang Conj. to target the bone and utilize it as a reservoir for sustaining a therapeutic plasma level of active peptide. High stability in solution and significant prolongation of Ang Conj. plasma half-life after *i.v.* and *s.c.* administration indicate our approach's effectiveness in improving peptide chemical and biological stability. The Ang Conj. bone-targeting ability and loading capacity on the bone resulted in a prolonged circulation half-life and higher efficacy than the native peptide. Overall, this study's results suggest that Ang Conj. is a promising therapeutic option for treating the activated RAS-associated inflammatory bone diseases such as osteoporosis, osteoarthritis, rheumatoid arthritis, Paget's disease, and cancers with bone metastasis.

Acknowledgements The authors want to thank Dr. Jared Barrott for his help in animal blood sampling and Mary van Muelken for her efforts in proofreading this manuscript.

Author contributions AAH did the study design, synthesis of Ang1–7 conjugate, animal dosing and sampling, tissue distribution and PK studies, drafting the manuscript. The stability study, HPLC analysis, HA binding study, data interpretation, data analysis, revising manuscript content, and approving the final version of the manuscript were made by AAH and SK.

Funding The authors did not receive support from any organization for the submitted work.

Availability of data and material (data transparency) The data and material will be available upon receipt of an official request.

Code availability (software application or custom code) Not applicable.

Declarations

Conflict of interest (include appropriate disclosures) The novel approach of conjugate synthesis was filed for a US patent application on July, 24, 2020, by the corresponding author. No author has an actual or perceived conflict of interest with the contents of this article.

Ethics approval (include appropriate approvals or waivers) The animal protocol No. 760 was approved by the Idaho State University Institutional Animal Care and Use Committee.

Consent to participate (include appropriate statements) Not applicable.

Consent for publication (include appropriate statements) Not applicable.

References

Carey RM, Padia SH (2018) Physiology and regulation of the renin–angiotensin–aldosterone system. In: Textbook of nephro-endocrinology. Elsevier, pp 1–25

Chen J-L, Zhang D-L, Sun Y, Zhao Y-X, Zhao K-X, Pu D, Xiao Q (2017) Angiotensin-(1–7) administration attenuates Alzheimer's disease-like neuropathology in rats with streptozotocin-induced diabetes via Mas receptor activation. Neuroscience 346:267–277

Cook KL, Metheny-Barlow LJ, Tallant EA, Gallagher PE (2010) Angiotensin-(1–7) reduces fibrosis in orthotopic breast tumors. Cancer Res 70:8319–8328

da Silveira KD et al (2010) Anti-inflammatory effects of the activation of the angiotensin-(1–7) receptor, MAS, in experimental models of arthritis. J Immunol 185:5569–5576

De Mello WC, Ferrario CM, Jessup JA (2007) Beneficial versus harmful effects of Angiotensin (1–7) on impulse propagation and cardiac arrhythmias in the failing heart. J Renin Angiotensin Aldosterone Syst 8:74–80

El-Hashim AZ, Renno WM, Raghupathy R, Abduo HT, Akhtar S, Benter IF (2012) Angiotensin-(1–7) inhibits allergic inflammation, via the MAS1 receptor, through suppression of ERK1/2-and NF-κB-dependent pathways. Br J Pharmacol 166:1964–1976

Fraker PJ, Speck JC Jr (1978) Protein and cell membrane iodinations with a sparingly soluble chloroamide, 1, 3, 4, 6-tetrachloro-3a, 6a-diphenylglycoluril. Biochem Biophys Res Commun 80:849–857

Gallagher P, Arter A, Deng G, Tallant E (2014) Angiotensin-(1–7): a peptide hormone with anti-cancer activity. Curr Med Chem 21:2417–2423

Giani JF et al (2009) Chronic infusion of angiotensin-(1–7) improves insulin resistance and hypertension induced by a high-fructose diet in rats. Am J Physiol-Endocrinol Metab 296:E262–E271

Giani JF et al (2012) Angiotensin-(1–7) attenuates diabetic nephropathy in Zucker diabetic fatty rats. Am J Physiol-Renal Physiol 302:F1606–F1615

Habashi AA, Khajehpour S, Ranjit A (2020) Prevention and treatment of rheumatoid arthritis using bone-targeted angiotensin peptide in rats. FASEB J. https://doi.org/10.1096/fasebj.2020.34.s1.02956 10.1096/fasebj.2020.34.s1.02956

Hamidi M, Azadi A, Rafiei P (2006) Pharmacokinetic consequences of pegylation. Drug Deliv 13:399–409

Iwanami J et al (2014) Role of angiotensin-converting enzyme 2/angiotensin-(1–7)/Mas axis in the hypotensive effect of azilsartan. Hypertens Res 37:616–620

Jevševar S, Kunstelj M, Porekar VG (2010) PEGylation of therapeutic proteins. Biotechnol J 5:113–128

Jiang T, Gao L, Guo J, Lu J, Wang Y, Zhang Y (2012) Suppressing inflammation by inhibiting the NF-κB pathway contributes to the neuroprotective effect of angiotensin-(1–7) in rats with permanent cerebral ischaemia. Br J Pharmacol 167:1520–1532

Jiang T et al (2016) Angiotensin-(1–7) is reduced and inversely correlates with tau hyperphosphorylation in animal models of Alzheimer's disease. Mol Neurobiol 53:2489–2497

Kangussu LM et al (2013) Angiotensin-(1–7) attenuates the anxiety and depression-like behaviors in transgenic rats with low brain angiotensinogen. Behav Brain Res 257:25–30

Klein N et al (2013) Angiotensin-(1–7) protects from experimental acute lung injury. Crit Care Med 41:e334–e343

Kluskens LD et al (2009) Angiotensin-(1–7) with thioether bridge: an angiotensin-converting enzyme-resistant, potent angiotensin-(1–7) analog. J Pharmacol Exp Ther 328:849–854

Ko B, Bakris G (2018) The renin–angiotensin–aldosterone system and the kidney. In: Textbook of Nephro-Endocrinology. Elsevier, pp 27–41

Krishnan B, Torti FM, Gallagher PE, Tallant EA (2013) Angiotensin-(1–7) reduces proliferation and angiogenesis of human prostate cancer xenografts with a decrease in angiogenic factors and an increase in sFlt-1. Prostate 73:60–70

Loot AE, Roks AJ, Henning RH, Tio RA, Suurmeijer AJ, Boomsma F, van Gilst WH (2002) Angiotensin-(1–7) attenuates the development of heart failure after myocardial infarction in rats. Circulation 105:1548–1550

Lula I et al (2007) Study of angiotensin-(1–7) vasoactive peptide and its β-cyclodextrin inclusion complexes: complete sequence-specific NMR assignments and structural studies. Peptides 28:2199–2210

Machado R, Santos R, Andrade S (2001) Mechanisms of angiotensin-(1–7)-induced inhibition of angiogenesis. Am J Physiol-Regulat Integrat Compar Physiol 280:R994–R1000

Petty WJ, Miller AA, McCoy TP, Gallagher PE, Tallant EA, Torti FM (2009) Phase I and pharmacokinetic study of angiotensin-(1–7), an endogenous antiangiogenic hormone. Clin Cancer Res 15:7398–7404

Petty WJ, Aklilu M, Varela VA, Lovato J, Savage PD, Miller AA (2012) Reverse translation of phase I biomarker findings links the activity of angiotensin-(1–7) to repression of hypoxia inducible factor-1α in vascular sarcomas. BMC Cancer 12:404

Pham H et al (2013) Pharmacodynamic stimulation of thrombogenesis by angiotensin (1–7) in recurrent ovarian cancer patients receiving gemcitabine and platinum-based chemotherapy. Cancer Chemother Pharmacol 71:965–972

Rodgers KE, Oliver J (2006) Phase I/II dose escalation study of angiotensin 1–7 [A (1–7)] administered before and after chemotherapy in patients with newly diagnosed breast cancer. Cancer Chemother Pharmacol 57:559–568

Santos RA (2014) Angiotensin-(1–7). Hypertension 63:1138–1147

Santos SHS et al (2010) Improved lipid and glucose metabolism in transgenic rats with increased circulating angiotensin-(1–7). Arterioscler Thromb Vasc Biol 30:953–961

Sasaki S, Higashi Y, Nakagawa K, Matsuura H, Kajiyama G, Oshima T (2001) Effects of angiotensin-(1–7) on forearm circulation in normotensive subjects and patients with essential hypertension. Hypertension 38:90–94

Shenoy V et al (2014) Oral delivery of Angiotensin-converting enzyme 2 and Angiotensin-(1–7) bioencapsulated in plant cells attenuates pulmonary hypertension. Hypertension 64:1248–1259

Silveira KD et al (2013) Beneficial effects of the activation of the angiotensin-(1–7) MAS receptor in a murine model of adriamycin-induced nephropathy. PLoS ONE 8:e66082

Soto-Pantoja DR, Menon J, Gallagher PE, Tallant EA (2009) Angiotensin-(1–7) inhibits tumor angiogenesis in human lung cancer xenografts with a reduction in vascular endothelial growth factor. Mol Cancer Ther 8:1676–1683

Souza LL, Costa-Neto CM (2012) Angiotensin-(1–7) decreases LPS-induced inflammatory response in macrophages. J Cell Physiol 227:2117–2122

Wester A, Devocelle M, Tallant EA, Chappell MC, Gallagher PE, Paradisi F (2017) Stabilization of Angiotensin-(1–7) by key substitution with a cyclic non-natural amino acid. Amino Acids 49:1733–1742

Yewle JN, Puleo DA, Bachas LG (2013) Bifunctional bisphosphonates for delivering PTH (1–34) to bone mineral with enhanced bioactivity. Biomaterials 34:3141–3149

Zhang J, Noble NA, Border WA, Huang Y (2010) Infusion of angiotensin-(1–7) reduces glomerulosclerosis through counteracting angiotensin II in experimental glomerulonephritis. Am Jo Physiol-Renal Physiol 298:F579–F588